High-efficiency E×B drifting electron laser with electrostatic wiggler

Spilios Riyopoulos
Science Application International Corporation, McLean, Virginia 22102
(Received 3 February 1997)

High power operation of an **E**×**B** drifting electron laser (DEL) with electrostatic (ES) wiggler offers the same advantages with the previously introduced magnetostatic wiggler (MS) version, namely, much higher efficiency than the free electron laser (FEL) $\eta \leqslant 1/2N_w$ limit, due to unrestricted particle excursions. A parameter scaling allows unified treatment of oblique radiation emission, space charge effects and sensitivity to beam thermal spreads, for both the ES and MS cases. Emission at an angle relative to the drifting beam occurs naturally in an ES wiggler, while tilting the resonator axis is proposed to compensate for the off-axis walk of the emitting electrons for finite radiation spot size. No efficiency loss occurs at small tilt angles. It is also shown that DEL's exhibit much higher tolerance to low beam quality than FEL's. Finally, the DEL operation at low radiation power, with finite trapped particle excursions, is analyzed. It is shown that the efficiency there can still exceed that of a comparable FEL, particularly at low wiggler strengths. [S1063-651X(97)02810-9]

PACS number(s): 52.75.Ms, 41.60.Cr

I. INTRODUCTION

In a drifting electron laser (DEL) a relativistic **E**×**B** drifting beam in orthogonal static electric and magnetic fields [1,2] is undulated by a periodic variation in either **E** or **B**. Though the relativistic frequency upshifting is the same as in a free electron laser [3–6] (FEL), the interaction mechanism is distinctively different. The emitted radiation energy and momentum come respectively from the change in the electrostatic energy $eE_0\delta X$ and vector potential $eB_0\delta X$ of the electron, δX being the recoil of the guiding center (GC) location perpendicular to the drift direction. Since the wave-particle resonance depends on the average electron drift velocity, $u=cE_0/B_0$, the change in the ES energy does not cause detuning.

Previous DEL studies focused on a magnetostatic (MS) wiggler configuration [1]. Because the wiggler strength must vary in the direction of the dc electric field, a separate wiggler magnet is needed orthogonal to the uniform B_0 magnet. For exactly the same reason, the periodic and the uniform potential are applied on the same direction in case of a DEL with electrostatic (ES) wiggler. Applying both the uniform and undulating voltage on the same structure, Fig. 1, offers advantages in compactness and number of magnets required.

The present paper discusses a DEL with electrostatic wiggler. It is shown that the resonant interaction comes from the beating of the *axial* (parallel to the beam velocity) components of the wiggler and the radiation field, as they appear in the moving frame, instead of the usual beating among the transverse wiggler-radiation fields occurring with an MS wiggler. Under equal ES and MS wiggler strengths $V_w=A_w$ the normalized strength a_w is higher by a factor $\gamma_u\beta_u$ in the ES case. The coupling strength also changes by a factor $\gamma_u^2\beta_u\sin\phi$; radiation is emitted at a small angle ϕ relative to the beam direction.

With the introduction of proper scaling factors, a similar dynamic description applies to both ES and MS wigglers. It has already been demonstrated that at high power operation, the electronic efficiency by far exceeds the FEL limit $1/2N_w$, N_w being the number of wiggler periods; there is no inverse gain-efficiency relation as in an FEL. A unified treatment is adopted here to address the issues related with oblique emission, space charge effects, sensitivity to beam quality, and efficiency at low power operation.

Oblique emission (at a small angle) naturally dominates in a ES wiggler. For large radiation spot size it is shown that no reduction in efficiency is caused by the oblique emission. In case of small radiation spot size, resonator tilting can be applied as a tapering mechanism for both wigglers, in order to maintain the spatial overlapping between radiation and the off-axis walking electrons.

It is shown that the space charge of a laminar beam has a similar effect with the gradient in the wiggler strength: they both create a shear in the **E**×**B** velocity of the beam. The magnitude of that shear, balanced again the focusing effect of the radiation, determines whether the particle excursions are unbound or not; island formation in the second case limits the efficiency. It is found that space charge effects are easier to overcome than the wiggler gradient effects.

While high efficiency with unbound electron excursions occurs at high radiation power $A_r > A_w$, the operation at low power reverts to trapped particle island formation and $1/N_w$ efficiency scaling [6] as in an FEL. That is true for an ES wiggler DEL as well, despite the originally expressed hope for the opposite [1]. Yet, depending on the operation parameters, the coefficient multiplying $1/2N_w$ can be much higher than unity, and the DEL efficiency, for both ES and EM wigglers, can still exceed that of a comparable FEL.

The sensitivity to beam quality is finally addressed. A

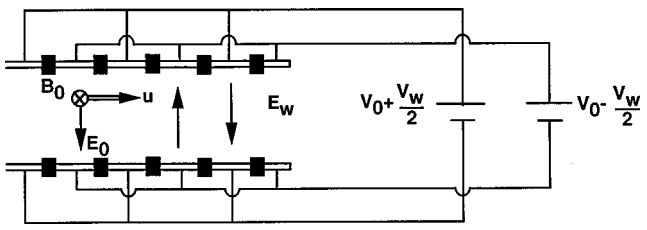

FIG. 1. Illustration of the drifting electron laser concept with an electrostatic wiggler.

velocity mismatch *per se* does not affect the resonant condition since the drift velocity is determined by $\mathbf{E}_0\times\mathbf{B}_0$. Thermal velocity spreads are converted into a shift of the GC position from the intended location, and give rise to finite Larmor radius. It is shown that the effect of thermal spreads on efficiency is much lower in a DEL and easier to overcome than in a comparable parameters FEL.

The rest of the analysis is divided as following. Section II introduces the field configuration and the basic operation principle for an ES wiggler. A general resonant interaction Hamiltonian for the slow time scale motion of the electron GC is derived in Sec. III in the frame moving at the drift velocity, unifying ES and EM treatment and including space charge effects. Section IV is dedicated to computing the nonlinear efficiency at saturation for a sheet beam as a function of the frequency detuning and the beam placement in the gap. Section V examines low power DEL operation when island formation takes place. Section VI discusses the sensitivity to thermal spreads and the effects of finite size radiation envelope. Section VI summarizes the results.

II. OPERATION PRINCIPLE FOR THE ES WIGGLER DEL

Schematic illustration of the electrostatic-wiggler DEL concept is shown in Fig. 1. The applied static fields are given by

$$\mathbf{B}=B_0\hat{\mathbf{y}},\quad \mathbf{E}=E_0\hat{\mathbf{x}}+E_w[\sinh(k_wx)\cos(k_wz)\hat{\mathbf{x}}-\cosh(k_wx)\sin(k_wz)\hat{\mathbf{z}}], \tag{1}$$

derived from the potentials

$$\mathbf{A}_0=B_{naught}x\hat{\mathbf{z}},\quad \Phi_0(x)=E_{naught}x. \tag{2a}$$

$$\mathbf{E}_\mathbf{w}=-\nabla\Phi_w,\quad \Phi_w=-V_w\cosh(k_wx)\cos(k_wz). \tag{2b}$$

In the notation of Eqs. (12) the uniform dc electric and magnetic fields are negative, $E_0=-E_{naught}$ and $B_0=-B_{naught}$, respectively, where the positive E_{naught} and B_{naught} signifies the field magnitudes. The arrangement was chosen so that the wiggler strength varies along the direction of the uniform static $E_0\hat{\mathbf{x}}$, a necessary condition in order to have significant gain. The uniform (i.e., spatially averaged) component of the applied dc voltage is $V_0=\Phi_0(D)-\Phi_0(-D)$ where $2D$ is the anode-cathode spacing. The interaction Hamiltonian is

$$H=\sqrt{m^2c^4+c^2\left[\mathbf{P}+\frac{e}{c}(\mathbf{A}_0+\mathbf{A}_r)\right]^2}-e\Phi_0-e\Phi_w, \tag{3}$$

where $-e$ is the electron charge and $\mathbf{P}=\mathbf{p}-(e/c)(\mathbf{A}_0+\mathbf{A}_\mathbf{r})$ is the canonical momentum.

The electron GC undergoes an $\mathbf{E}_\mathbf{w}\times\mathbf{B}_0$ oscillation, on top of the Laminar $\mathbf{E}_0\times\mathbf{B}_0$ velocity, and undulates on the xz plane perpendicular to the uniform magnetic field. The emitted radiation is also polarized in the xy plane. Direct coupling between the wiggling motion and the radiation (producing the ''beating'' term $\mathbf{A}_\mathbf{w}\cdot\mathbf{A}_\mathbf{r}$), is achieved when the radiation is emitted at a small angle ϕ relative to the (unperturbed) beam velocity (Fig. 2),

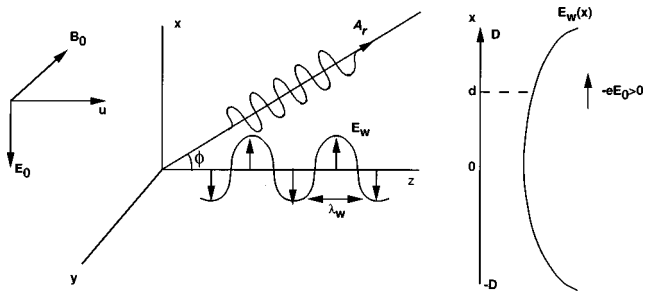

FIG. 2. Illustration of the geometry and field arrangement in a DEL with electrostatic wiggler.

$$\mathbf{A}_\mathbf{r}=A_r\begin{pmatrix}\cos\phi\hat{\mathbf{x}}\\0\\\sin\phi\hat{\mathbf{z}}\end{pmatrix}\sin(k_{rx}x+k_{rz}z-\omega_rt), \tag{4a}$$

$$\mathbf{k}_\mathbf{r}=\begin{pmatrix}k_{rx}\\0\\k_{rz}\end{pmatrix}=\begin{pmatrix}\sin\phi\\0\\\cos\phi\end{pmatrix}k_r. \tag{4b}$$

There is also indirect coupling between undulation and radiation, mediated by the cyclotron motion; the coupling strength is smaller by a factor $k_w\rho$, a small number for DEL operation, relative to the direct coupling. Only the small indirect coupling remains at exactly parallel emission $\phi=0$; direct coupling dominates above a small angle $\tan\phi>k_w\rho$.

Since no force is acting in the y direction the canonical momentum P_y is a constant of motion that is set to zero,

$$P_y=p_y=0. \tag{5}$$

The interaction responsible for the lasing action follows from the equations of motion in the other two directions xz are

$$\frac{d\mathbf{v}}{dt}=-\frac{e}{\gamma m}\left(\mathbf{E}+\frac{\mathbf{v}\times\mathbf{B}}{c}\right)-\mathbf{v}\frac{1}{\gamma}\frac{d\gamma}{dt}, \tag{6}$$

where the rate of change of the energy is given by

$$mc^2\frac{d\gamma}{dt}=-e\mathbf{v}\cdot\mathbf{E}. \tag{7}$$

The GC of the cyclotron rotation for an ''unperturbed'' electron drifts along z with average $\mathbf{E}_0\times\mathbf{B}_0$ velocity $\mathbf{u}=cE_0/B_0\hat{\mathbf{z}}$; at the same time, it undergoes an $\mathbf{E}_\mathbf{w}\times\mathbf{B}_0$ undulation in the xz plane due to the periodic wiggler action $\mathbf{E}_\mathbf{w}$. The transverse wiggling velocity v_{x0} interacts with the radiation magnetic field B_{1y} to produce an axial force $f_{1z}=ev_{x0}B_{1y}/c$. Application of the axial force on a particle gyrating about B_{0y} causes the GC of the gyration to drift along x, i.e., in the direction perpendicular to both f_{1z} and B_{0y}. The subsequent change in the particle potential energy $\delta(-e\Phi_0)=-eE_{naught}\delta x$ is converted into radiation energy. The change in the electron canonical momentum, associated with the vector potential $\delta P_z=\delta(-eA_{y0}/c)=-m\Omega\delta x$, is converted to radiation momentum. The cyclotron rotation energy is also frozen, since no cyclotron resonance is involved. Hence the particle kinetic energy and momentum remain invariant during radiation emission.

More specifically, the energy-momentum conservation during a photon emission/absorption at an angle ϕ relative to the beam direction yields [7]

$$-m\Omega\,\delta X=\mp\hbar(k_w+k_r\cos\phi), \tag{8a}$$

$$-eE_{naught}\delta X=\mp\hbar\,\omega_r, \tag{8b}$$

where $\Omega=eB_{naught}/mc$. Dividing Eq. (8b) by Eq. (8a) to eliminate δX, and using $u=eE_{naught}/m\Omega$ for the $\mathbf{E}_0\times\mathbf{B}_0$ drift velocity, yields the DEL operation resonance

$$\omega_r-(k_w+k_r\cos\phi)u=0, \tag{9}$$

with resonant emission frequency

$$\omega_r=\left(1+\frac{u}{c}\cos\phi\right)\overline{\gamma_u^2}k_w u, \tag{10}$$

where $\overline{\gamma_u^2}=\sqrt{1-\cos^2\phi u^2/c^2}$. For $u\simeq c$ and given that $\cos\phi\sim 1/\overline{\gamma_u}\ll 1$, Eq. (10) yields $\omega_r\simeq 2\gamma_u^2 k_w c$, corresponding to the frequency of an FEL with beam velocity equal to the zeroth-order drift u. The difference from an FEL is that, according to Eq. (8b), it is the electrostatic, rather than the kinetic energy, being converted to radiation. Also, there is no cyclotron resonance involved in Eq. (9) and therefore no energy exchange takes place with the cyclotron rotation about the drifting GC, distinguishing the DEL from a cyclotron maser [8].

In the ES wiggler DEL the radiation electric field lies on the same plane with the cyclotron rotation (Fig. 2), causing direct coupling of the gyromotion with the radiation (in a MS wiggler DEL the radiation electric field is perpendicular to the plane of gyration). As a result, emission is also possible at the drift-cyclotron resonances defined by

$$\omega_r-k_r\cos\phi_u\mp\frac{n\Omega}{\gamma_u^2}=0, \tag{11}$$

Finally, in both ES and MS wigglers emission also occurs at the wiggler-cyclotron hybrid frequency

$$\omega_r-(k_w+k_r\cos\phi)u\mp\frac{n\Omega}{\gamma_u^2}=0, \tag{12}$$

which is the relativistic upshift of the sum of the wiggler plus the cyclotron (harmonic) frequency. When cyclotron harmonics are involved both ES plus cyclotron rotation energy are converted to radiation, necessitating separate treatment of the DEL operation at $n\neq 0$. The present analysis deals with operation at the fundamental $n=0$, Eq. (9).

The DEL operation principle is more similar to that of crossed-field devices [9,10] (magnetrons) where a slow wave $v_p\ll c$ ''caviton'' is emitted by a drifting electron; here the emission of a photon $v_p=c$ requires the mediation of the wiggler k_w to satisfy momentum conservation. In both devices the linear gain is proportional to the transverse spatial derivative of the stimulated emission probability [7,11], as opposed to the frequency derivative entering the FEL linear gain. Therefore, in both devices the linear [7,11] and nonlinear [1,10] gains are found symmetric relative to the frequency detuning from resonance, contrasting the antisymmetric gain vs frequency [3–6] for FEL's. Because of the dependence on the transverse spatial gradient, the basic DEL theory is necessarily two dimensional; one dimension suffices to describe the basic FEL interaction. The DEL gain is antisymmetric relative to the beam displacement from the center of the cavity.

III. RESONANT PARTICLE MOTION IN THE DRIFTING FRAME

It is simpler to consider the particle motion in the frame moving at the $\mathbf{E}_0\times\mathbf{B}_0$ drift velocity where the Lorenz transformed dc electric field E'_{0x} is zero, and the unperturbed electron motion is a cyclotron rotation with constant Larmor radius about an oscillating GC [in the lab frame the gyration appears elliptic due to the Lorenz length contraction in the z direction; the gyroradius varies with the gyroangle $\rho\rightarrow\rho(\theta)$ complicating Bessel function expansions]. The energy exchange in the lab frame will eventually be expressed in terms of the drifting frame coordinates, exploiting the four-vector covariance of $\mathbf{v}\cdot\mathbf{E}$.

The drifting frame quantities, labeled by a prime, are related with the lab frame (unprimed) quantities as

$$E'_{0x}=\gamma_u\left(E_{0x}-\frac{u}{c}B_{0y}\right)=0,$$

$$B'_{0y}=\gamma_u\left(B_{0y}-\frac{u}{c}E_{0x}\right)=\frac{B_{0y}}{\gamma_u}, \tag{13}$$

$$A'_r\equiv\begin{pmatrix}\mathcal{A}'_{rx}\\0\\\mathcal{A}'_{rz}\end{pmatrix}=\begin{pmatrix}\mathcal{A}_{rx}\\0\\\gamma_u\mathcal{A}_{rz}\end{pmatrix}$$

$$=A_r\begin{pmatrix}\cos\phi\\0\\\gamma_u\sin\phi\end{pmatrix}\sin(k'_{rx}x'+k'_{rz}z'-\omega'_r t'),$$

$$\Phi'_r=-\gamma_u\frac{u}{c}\mathcal{A}_{rz}$$

$$=-\gamma_u\frac{u}{c}A_r\sin\phi\sin(k'_{rx}x'+k'_{rz}z'-\omega'_r t'), \tag{14a}$$

$$\Phi'_w=\gamma_u\Phi_w=-\gamma_u V_w\cosh(\kappa_w x')\cos(k'_w z'-\omega'_w z'),$$

$$\mathcal{A}'_{wz}=-\gamma_u\frac{u}{c}\Phi_w=\gamma_u\frac{u}{c}V_w\cosh(\kappa_w x')\cos(k'_w z'-\omega'_w z'), \tag{14b}$$

where $V_w=k_w^{-1}E_w$ and use was made of the scalar invariance of the phase $\mathbf{k}\cdot\mathbf{r}-\omega t$. The following notation is introduced: $\mathbf{A}$ for a vector and $\mathcal{A}$ for its vector components (both amplitude and phase), while A signifies just the amplitude. Notice that the Lorenz transformations mix electrostatic (Φ) and axial vector potential ($\mathcal{A}_z$) components so that the ES wiggler potential in the lab frame generates a vector potential

component in the drifting frame; the latter produces the direct coupling between wiggler undulation and radiation in the particle interaction Hamiltonian which will follow. The frequencies and wave numbers transform according to [12]

$$\begin{pmatrix} k'_{rx} \\ 0 \\ k'_{rz} \end{pmatrix} = \begin{pmatrix} k_r \sin\phi \\ 0 \\ \gamma_u k_r(\cos\phi - \beta_u) \end{pmatrix}, \quad \omega'_r = \gamma_u(\omega_r - k_r u\ \cos\phi), \tag{15a}$$

$$\kappa'_w = k_w, \quad k'_w = \gamma_u k_w, \quad \omega'_w = \gamma_u(-k_w u), \tag{15b}$$

and $\Omega' = \Omega/\gamma_u$, where $\beta_u = u/c$ and $\gamma_u = \sqrt{1-(u/c)^2}$. Applying transformations (14) to the resonant condition (9) it follows that [12]

$$k'_{rz} = \beta_u \frac{\cos\phi - \beta_u}{1 - \cos\phi\beta_u} k'_w. \tag{16}$$

Hence for small $\sin\phi \sim \epsilon \ll 1$, $\cos\phi \sim 1 - \epsilon^2$, one has $k'_{rz} \simeq k'_w$ in the drifting frame.

Employing expressions (13)–(15) for the fields, the interaction Hamiltonian in the drifting frame is given by

$$H' = \sqrt{m^2c^4 + c^2[(P'_x + e\mathcal{A}'_{rx})^2 + (P'_z + m\Omega' x' + e\mathcal{A}'_{wz} + e\mathcal{A}'_{rz})^2]} - e\Phi'_w - e\Phi'_r. \tag{17}$$

Ordering according to the small parameters $P'_\perp/mc \sim eA_r/mc^2 \sim eA_w/mc^2 \sim \mathcal{O}(\epsilon) \ll 1$ the drifting frame Hamiltonian is expanded as $H' = H'_0 + H'_1$. Here

$$H'_0 = \sqrt{m^2c^4 + c^2[P_x'^2 + (P'_z + m\Omega' x')^2]} - e\Phi'_w - e\Phi'_r = mc^2\gamma'_\perp - e\Phi'_w - e\Phi'_r, \tag{18}$$

involves the integrable part (relativistic cyclotron motion) plus first order terms in ϵ; the second order

$$H'_1 \simeq \frac{1}{2\gamma'_\perp m}\left[2P'_x \frac{e}{c}\mathcal{A}'_{rx} + 2(P'_z + m\Omega' x')\left(\frac{e}{c}\mathcal{A}'_{rz} + \frac{e}{c}\mathcal{A}'_{wz}\right) + 2\frac{e}{c}\mathcal{A}'_{wz}\frac{e}{c}\mathcal{A}'_{rz} + \left(\frac{e}{c}\mathcal{A}'_{wz}\right)^2 + \left(\frac{e}{c}\mathcal{A}'_{rz}\right)^2\right] \tag{19}$$

describes the pairwise interactions among cyclotron rotation, undulation and radiation. After a cyclotron expansion of Eq. (19) it is clear that only the product $\mathcal{A}'_{wz}\mathcal{A}'_{rz}$ involving the beating of the wiggler and radiation vector potentials, corresponds to resonant interaction at the DEL frequency (9). The rest of the terms correspond to resonances (11) and (12) with Doppler-shifted cyclotron (harmonics), far from the operation frequency.

There are two time scales involved in the motion. The undulation period $\tau'_w \simeq 1/\omega'_w$ and the cyclotron oscillation period $\tau'_c \sim 1/\Omega'$ are much shorter than the characteristic time $D(dX/dt)^{-1}$ of the resonant interaction. To take advantage of the separation in temporal and spatial scales we switch into the GC coordinates

$$x' = X' + \rho'\sin\theta', \quad P'_x = -m\Omega'\rho'\cos\theta', \tag{20}$$

$$z' = Z' + \rho'\cos\theta', \quad P'_z = -m\Omega' X',$$

where X', Z' define the GC location, $\rho' = (-2I'/m\Omega')^{1/2}$ is the Larmor radius, and θ' is the cyclotron angle. A fast-time averaging of the transformed $H'(I', \theta', X', Z')$, yields (Appendix A) the slow-time scale Hamiltonian

$$H'_R = mc^2\overline{\gamma'_\perp} + \frac{mc^2 a_w a_r}{2\overline{\gamma'_\perp}}\gamma_u^2\beta_u \sin\phi\cosh(\kappa'_w X')\times\sin(K'\Psi' + k'_{rx}X') - \frac{\Delta'_\omega}{K'}m\Omega' X', \tag{21}$$

$$\overline{\gamma'_\perp}(X') = \sqrt{1 + \beta_\perp'^2 + \frac{1}{4}\gamma_u^2\beta_u^2\left(\frac{eV_w}{mc^2}\right)^2(1 + \cosh[2k'_w X'])}, \tag{22}$$

where $\beta'_\perp = (-2\Omega' I'/mc^2)^{1/2} = \Omega'\rho'/mc$ is a constant of motion. The ponderomotive phase in Eq. (21) depends on both X and Z positions through

$$\Psi' = Z' - \Delta'_\omega t'/K', \tag{23}$$

where

$$K' \equiv k'_w + k'_{rz} \simeq 2k'_w, \quad \Delta'_\omega \equiv \omega'_r + \omega'_w. \tag{24}$$

Using the relativistic transformations (15) inside Eq. (24), we see that $\Delta'_\omega = \gamma_u\Delta_\omega$, where

$$\Delta_\omega = \omega_r - (k_r\cos\phi + k_w)u \tag{25}$$

is the detuning from synchronism observed in the lab frame. The orbits in the drift frame are given by $H'_R = \text{const}$. At exact synchronism, $\Delta_\omega = 0$, the GC motion is an $E \times B$ drift along the ponderomotive equipotentials that appear ''frozen'' in the drifting frame.

The effect of the space-charge field from a laminar beam is easily superimposed on Eq. (21). The beam self-potential, viewed in the frame moving with the drift velocity u_0 at the beam center $X = d$, adds the contribution $(1/2)\gamma_u\omega_b^2(X-d)^2$ to the interaction energy. Hence, the generic Hamiltonian for oblique emission with either EM or ES wigglers, including the equilibrium space-charge effects, is given by

$$H'_R = mc^2\overline{\gamma'_\perp} + mc^2\mathcal{A}\cosh(\kappa'_w X')\sin(K'\Psi' + k'_{rx}X') - \frac{\Delta'_\omega}{K'}m\Omega' X' - \frac{1}{2}\gamma_u\omega_b^2(X'-d)^2, \tag{26}$$

$$\gamma'_\perp = \sqrt{1 + \beta_\perp'^2 + \overline{a_w'^2}(X')},$$

$$\overline{a_w^2}(X') = \frac{1}{4}\, a_w^2 (1+\cosh[2k_w' X']). \tag{27}$$

Expression (26) is similar to that in a MS wiggler DEL. It can be used for a unified treatment of both an ES and an MS wiggler DEL emitting at an angle ϕ under the following symbol definitions, respectively:

$$\mathcal{A} = \frac{a_w a_r}{2\overline{\gamma_\perp'}}\, \gamma_u \sin\phi, \quad a_w = \gamma_u \beta_u \left(\frac{eV_w}{mc^2}\right), \tag{28a}$$

$$\mathcal{A} = \frac{a_w a_r}{2\overline{\gamma_\perp'}} \cos\phi, \quad a_w = \left(\frac{eA_w}{mc^2}\right). \tag{28b}$$

The difference in coupling strengths $\mathcal{A}$ reflects the fact that interaction in the ES wiggler occurs through the beating of the axial (parallel to the beam) wiggler and radiation $E_r \sin\phi$ fields; the transverse components, $E_r \cos\phi$, are involved in an MS wiggler. For equal wiggler strengths $V_w = A_w$, the normalized ES strength a_w exceeds the corresponding MS by $\gamma_u \beta_u$. Under equal a_w, the operation with MS and ES wigglers is roughly equivalent when the coupling strengths $\mathcal{A}$ are equal, that is for emission at an angle $\gamma_u = \cot\phi$. At high γ_u emission is nearly parallel $\phi \ll 1$.

The general slow-time equations of motion are

$$\frac{dX'}{dt} = mc^2 \mathcal{A}\, \frac{K'}{m\Omega'} \cosh(\kappa_w' X') \cos(K'\Psi' + k_{rx}' X'), \tag{29a}$$

$$\frac{d\Psi'}{dt} = -mc^2 \mathcal{A} \left[\frac{\kappa_w'}{m\Omega'} \sinh(\kappa_w' X') \sin(K'\Psi' + k_{rx}' X') + \frac{k_{rx}'}{m\Omega'} \cosh(\kappa_w' X') \cos(K'\Psi' + k_{rx}' X') \right] + \frac{\Delta_\omega'}{K'} - \frac{c^2}{2\gamma_\perp' \Omega'} \frac{\partial \overline{a_w^2}}{\partial X'} - \gamma_u \frac{\omega_b^2}{\Omega'} (X' - d). \tag{29b}$$

The wiggler strength gradient and the space-charge potential act in a similar way: they cause a shear in the drift velocity, given, respectively by the third and fourth term in Eq. (29b). It is the magnitude of that shear that will determine whether the trapped particle motion is unbounded or bounded.

For $a_r < a_w$, the shear in the drift velocity leads to finite excursion and island formation. At high radiation power $a_r > a_w$ (and for a uniform radiation amplitude $da_r/dX = 0$ across the cavity), the typical phase space topology, plotted in Figs. 3(a) and 3(b) exhibits unbound orbits intercepting the plates. Unlike the nonlinear pendulum-type trapped particle orbits in an FEL, characterized by a finite size trapped island $\delta X \propto (a_w a_r)^{1/2}$, here both fixed points are unstable and the excursion δX transverse to the wave propagation is unbounded. The difference between Figs. 3(a) and 3(b) is low and high detuning Δ_ω, respectively. In Fig. 3(a) the phase of all electrons is trapped and the motion of trapped particles (shaded) is not bounded; given enough time they will be intercepted at $\pm D$. In Fig. 3(b) streaming particles appear; the motion of these particles oscillates about an average location X, and the average contribution to energy exchange is nearly zero (but not exactly because up and down excursions are not symmetric).

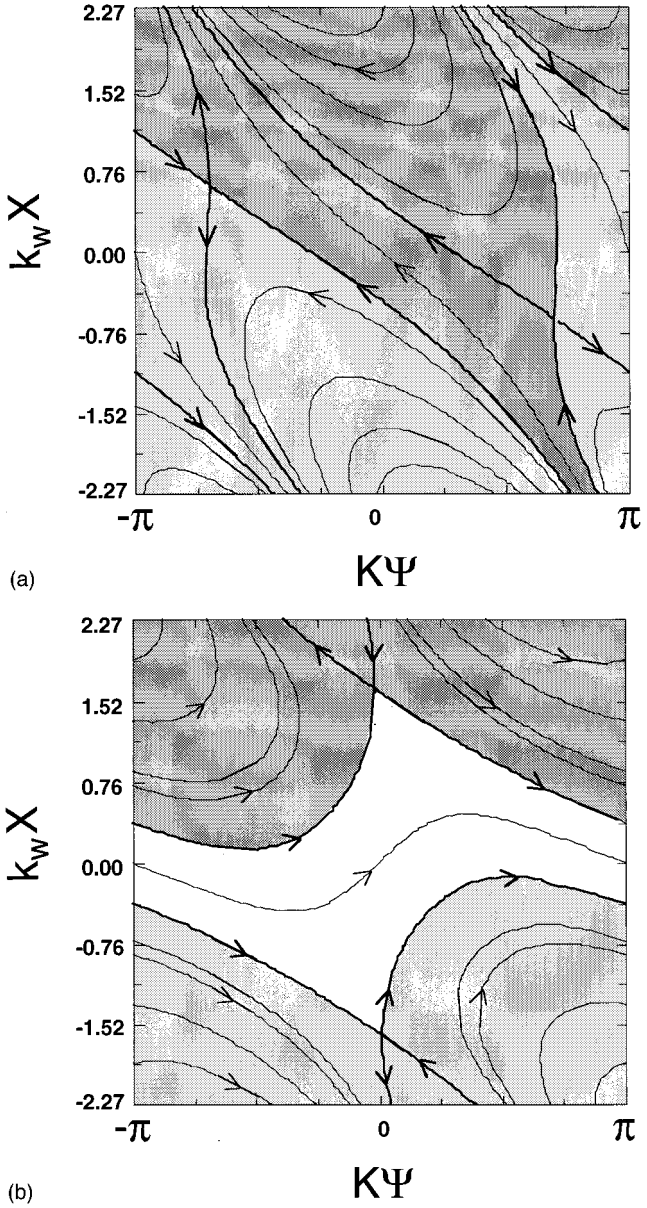

FIG. 3. Typical GC orbits, viewed in the drifting frame, for uniform radiation amplitude and emission angle $\phi = 0.5°$, showing unbound trapped particle excursions (no island formation) (a) ξ below critical detuning and (b) ξ above critical detuning.

IV. LARGE SIGNAL EFFICIENCY UNDER OBLIQUE EMISSION

The computation of the wave-particle energy exchange, performed in Ref. [1], shows that the total radiated energy from N_e electrons is related to the change in the GC potential energy by

$$\delta W_r = N_e e E_0 \langle \delta X \rangle = N_e \frac{\langle \delta X \rangle}{2D}\, eV_0. \tag{30}$$

The emitted radiation energy equals the change in the potential energy of the beam center of charge $\langle X\rangle = N_e^{-1}\Sigma X_i$, and amounts to a fraction $\langle \delta X\rangle/2D$ of the total dc potential V_0. In addition, the charge redistribution in the interaction space induces image currents on the anode-cathode plates; the dc source consumes an energy amount equal to the radiated energy in maintaining the fixed voltage,

$$\delta W_0 = N_e e E_{naught}\langle \delta X\rangle = N_e \frac{\langle \delta X\rangle}{2D} eV_0. \tag{31}$$

The injected beam energy is $W_b = N_e V_b$, where the beam voltage is defined by the kinetic energy $eV_b = (\gamma_u - 1)mc^2$ assuming that all electrons are injected exactly at the $\mathbf{E}_0 \times \mathbf{B}_0$ velocity. Dividing the radiated energy by the sum $\delta W_0 + W_b$, yields the electronic efficiency as

$$\eta = \frac{\delta W_r}{\delta W_0 + N_e e V_b} = \frac{(\langle \delta X\rangle/2D)(V_0/V_b)}{1 + (\langle \delta X\rangle/2D)(V_0/V_b)}. \tag{32}$$

The efficiency is determined by the ratios $\langle \delta X\rangle/2D$ and V_0/V_b. The efficiency is large for unbound excursions; then one can have $\langle \delta X\rangle/2D \simeq 1/2$ and $\eta \simeq 33\%$ for a moderate value $V_0/V_b \simeq 2$.

Most of the radiated energy comes from trapped particles, whose excursions are unbound and so, given enough interaction length, they can cross the full cavity gap. The streaming particle excursions are nearly symmetric about the injected location and average to zero. The space boundaries between streaming and trapped particles are the separatrix curves, i.e., the trajectories passing through the (unstable) fixed points X_0', Ψ_0', zeros of $dX'/dt' = d\Psi'/dt' = 0$, Eqs. (29a). Neglecting the shear terms, of order a_w^2, compared to $a_w a_r$, yields

$$\kappa_w' X_0' = \pm \sinh^{-1}(\xi),$$

$$K'\Psi_0' = \pm \mathrm{sgn}(\xi)\frac{\pi}{2} - k_{rx}' X_0' = \pm \mathrm{sgn}(\xi)\frac{\pi}{2} \mp \frac{1}{\gamma_u}\frac{\sin\phi\beta_u}{1-\beta_u\cos\phi}\sinh^{-1}(\xi), \tag{33}$$

where the detuning parameter ξ is defined by

$$\xi = \frac{\Delta_\omega' \Omega'}{\mathcal{A}c^2(k_{rz}' + k_w')\kappa_w'} = \frac{\Delta_\omega \Omega}{2\mathcal{A}\gamma_u c^2 k_w^2}. \tag{34}$$

All particles are trapped in the ''ponderomotive'' potential over a finite range of detuning $-\xi_c < \xi < \xi_c$. Streaming (untrapped) particles first appear at the middle of the gap $X' = 0$ (where the wiggler strength is minimum) when $|\xi| > \xi_c$. The critical detuning value marks the transition from the topology of Fig. 3(a) to that of Fig. 3(b) and the critical value equation

$$\sqrt{1+\xi_c^2} = \xi_c \sinh^{-1}\xi_c, \tag{35}$$

obtained in Ref. [1], yields the critical detuning value $\xi_c = 1.5088$.

The gain and efficiency are now computed for a monoenergetic sheet beam of fixed $\gamma_\perp$ (notice that γ_u is automatically set by the $\mathbf{E}_0 \times \mathbf{B}_0$ drift). The guiding centers of the injected electrons are located at $X = d$ and distributed uniformly along Ψ'. We are interested in the fraction of trapped particles moving upwards in X, marked by the heavy-shaded area in Figs. 3(a) and 3(b) releasing potential energy as radiation. Following Ref. [1], the upward fraction equals the width of the line segment $X = d$ inside the heavy shaded area of Fig. 3(b), divided by 2π,

$$f_{\mathrm{up}} = \frac{K'\Psi_+' - K'\Psi_-'}{2\pi}. \tag{36}$$

For $|\xi| < \xi_c$ the end points of the segment are given by

$$\sin(K'\Psi_\pm' + k_{rx}' d) = \frac{\pm\sqrt{1+\xi^2} - \xi[\pm\sinh^{-1}\xi - \kappa_w' d]}{\cosh(\kappa_w' d)}, \tag{37}$$

At saturation, the average GC excursion of the upward trapped electrons equals the beam-cathode separation $\langle \delta X\rangle = D - d$ and, according to Eq. (32), the energy released as radiation is

$$\delta W_r = -\left[f_{\mathrm{up}}\frac{D-d}{2D} - (1-f_{\mathrm{up}})\frac{D+d}{2D}\right] eV_0. \tag{38}$$

The second term subtracts the energy absorbed by particles moving downwards, since we have assumed that the radiation fills the space. For detuning increased above $|\xi| > \xi_c$ the emerging streaming particles about the midplane $X = 0$, separate two trapped populations. The trapped particles above and below the midplane lead to net radiation gain or net absorption, respectively. The new end-points for the upwards trapped fraction [heavy shaded area in Fig. 3(b)] are $K'\Psi_+'$, $K'\Psi_-' = -(\pi + K'\Psi_+')$, where

$$\sin(K'\Psi_+' + k_{rx}' d) = \frac{\sqrt{1+\xi^2} - \xi[\sinh^{-1}\xi - \kappa_w' d]}{\cosh(\kappa_w' d)}. \tag{39}$$

The energy released as radiation is

$$\delta W_r = -\,\mathrm{sgn}(d) f_{\mathrm{up}}\frac{D-d}{2D} eV_0. \tag{40}$$

In both Eqs. (38) and (40) the beam must be placed above the midplane $d > 0$ for gain.

According to Eqs. (37) and (39), the end points of the beam segment inside the shaded area shift by the same amount $k_{rx}' d$ relative to the parallel emission case $k_{rx}' = 0$. Hence, the trapped particle fraction, as well as the efficiency in terms of detuning, is given by the same function of the detuning ξ as in $\phi = 0$. The emission angle ϕ modifies ξ for given frequency mismatch Δ_ω.

The upward trapped fraction is symmetric in detuning, meaning that the same gain results at opposite frequency mismatches $\pm\Delta_\omega$ for given beam location d. The frequency symmetry $G(-\Delta_\omega) = G(\Delta_\omega)$ contrasts the antisymmetric gain for an FEL, and reflects the dynamical symmetry of the phase space; the GC flow patterns corresponding to opposite

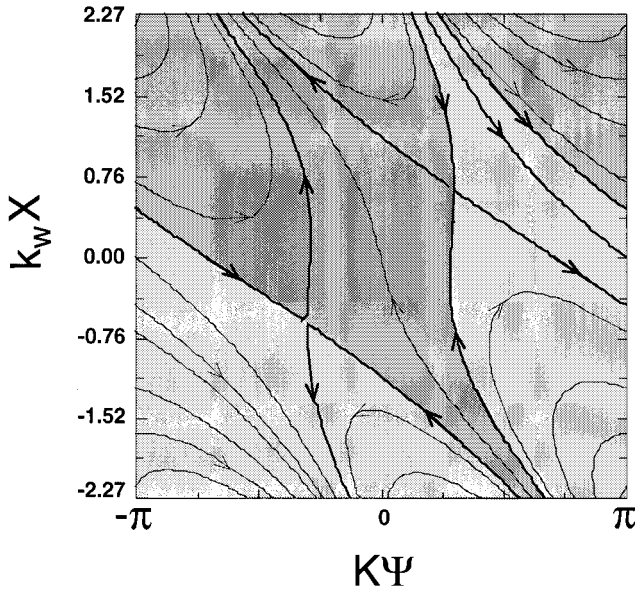

FIG. 4. Structure of the GC streamlines for the opposite detuning of Fig. 3(b). The reflection symmetry of the phase space around $\Psi' = 0$ generates the gain symmetry relative to detuning reversal.

detunings are mirror-symmetric relative to reflection around the $\Psi' = 0$ plane [compare Figs. 3(a) and 4]. Instead, for fixed detuning, the DEL gain is antisymmetric in the beam placement relative to the gap middle $d = 0$; opposite beam locations correspond to opposite gains $G(-d) = -G(d)$.

Level curves of the efficiency η from Eqs. (38)–(40) are plotted in $k_w d - \xi$ space in Fig. 5 for $\mathcal{V}_0 / V_b = 2$ inside an *A*-*K* gap $k_w D = 2.25$. There is a wide range of detuning ξ where the electronic efficiency is better than half the maximum efficiency of 55% obtained at $k_w d \simeq 0.7$, $\xi \simeq 1.6$. That demonstrates the small sensitivity of the gain to thermal spreads and the injected GC location, as well as the high

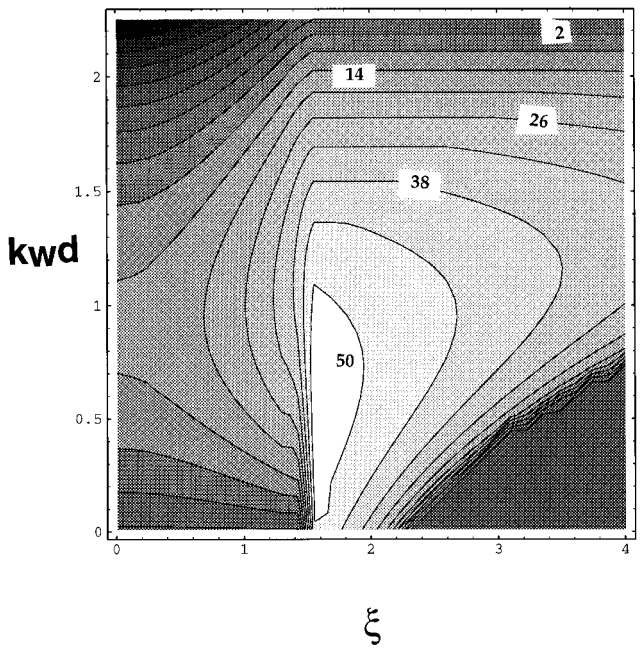

FIG. 5. Level plots of efficiency in $k_w d - \xi$ space. Here $k_w D = 2.25$ and $\mathcal{V}_0 / V_b = 2$.

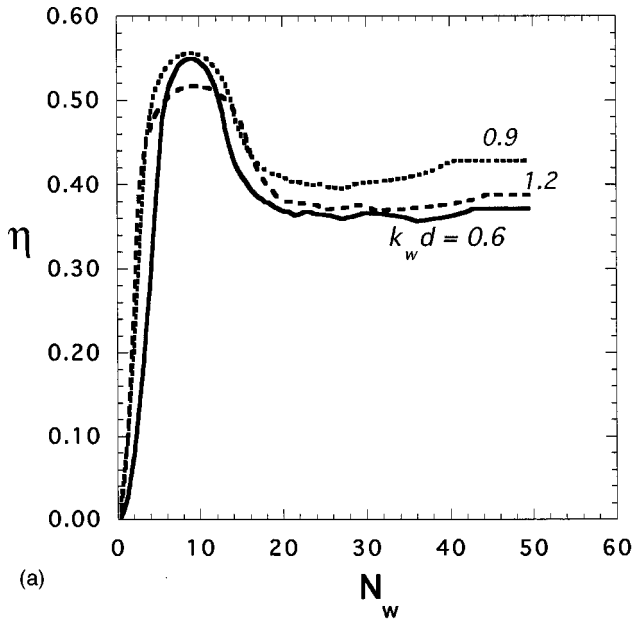

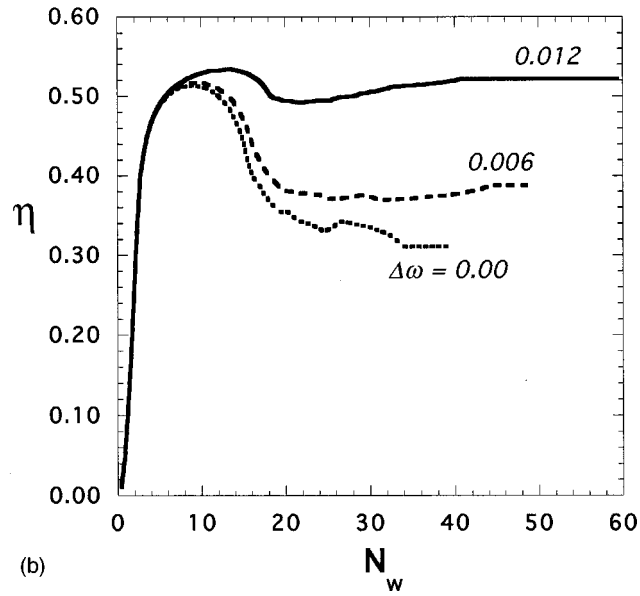

FIG. 6. Sheet beam efficiency vs number of wiggler periods N_w for $\mathcal{V}_0 / V_b = 2$, $k_w D = 2.25$, $u/c = 0.99$, $\phi = 0.5°$, and $a_w a_r = 10^{-2}$. (a) Various beam placements in the gap for $\xi = 0$ and (b) various detuning values for beam placed at $k_w d = 0.90$.

bandwidth capability of a DEL amplifier. The optimum beam placement is a compromise between maximizing the upwards trapped fraction $f_{\rm up}$ at $d \sim D$ and maximizing the per particle extracted energy that is proportional to the traveled distance $D - d$. The optimum beam placement d^* is independent of the external voltage, depending only on the ratio $k_w D$ of the anode-cathode gap to wiggler wavelength.

The efficiency vs the number of wiggler periods N_w, obtained by numerical integration of Eqs. (29), is plotted in Figs. 6(a) and 6(b) for some typical values of frequency detuning and beam placement in the gap, and for $\mathcal{V}_0 / V_b = 2$ inside an *A*-*K* gap $k_w D = 2.25$. In all curves the efficiency approaches quickly the corresponding saturation values, marked inside the level plot of Fig. 5; for this particular example, assuming an interaction strength $a_w a_r = 10^{-2}$ saturation occurs after only 10–15 wiggler periods.

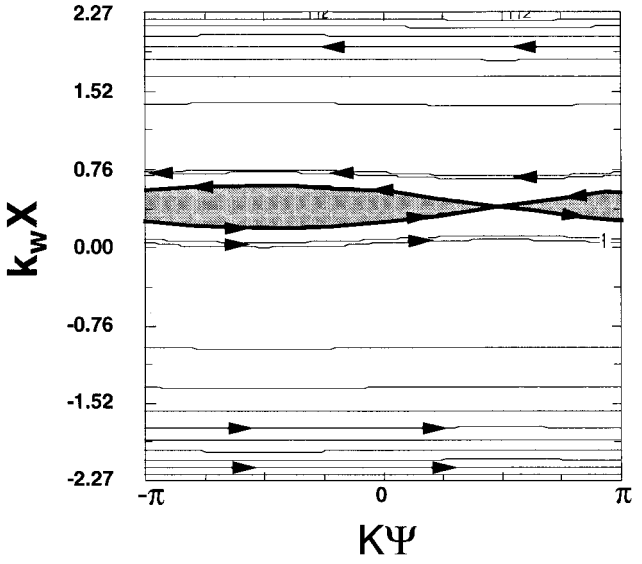

FIG. 7. Trapped particle orbits, in the drifting frame, for low radiation amplitude.

Though the results in Figs. 5 and 6 are obtained for constant radiation amplitude along the wiggler, inclusion of the self-consistent evolution of A_r would not reduce the efficiency. Since particles do not ''turn around the bucket'' in X, the DEL efficiency is not affected by the relation between wiggler length and bounce period; there is no concern of ''overshooting'' from a decrease in the bounce period caused by an increase in A_r. In fact, for given frequency mismatch, an increase in a_r reduces the effective detuning ξ, Eq. (34), and increases the trapped particle fraction in Fig. 3(b) [it has no effect in Fig. 3(a)]. Given enough interaction length the DEL efficiency tends to the saturation efficiency; the saturation length itself decreases as the radiation power increases.

V. EFFICIENCY AT LOW POWER OPERATION

At low radiation power, roughly $a_r < a_w$, particles in resonance get trapped in islands, Fig. 7. The maximum particle excursion is limited by the separatrix height, which in turn, depends on the radiation amplitude. Two consequences follow: the electronic efficiency is reduced, and it now depends on the relation between interaction length and the electron ''bounce period'' around the island. The optimum efficiency scales inversely proportional to the optimum interaction length $1/L_w$ just as in an FEL. In a DEL, however, the coefficient multiplying $1/L_w$ can be higher than unity, thus still allowing higher than FEL efficiency.

The stability equations for small perturbations $\delta X \equiv X' - X'_0$, $\delta\zeta' \equiv \zeta' - \zeta'_0$ about the fixed points yield the eigenvalue equation (Appendix B)

$$\lambda_{\pm}^2 = (H_{X\Psi}^2 - H_{XX}H_{\Psi\Psi})/m^2\Omega'^2, \tag{41}$$

where the $\pm$ sign corresponds to $k'_{rz}\Psi'_0 = \pm\pi/2$, $-k'_{rx}X'_0$ respectively. Substituting the derivatives at X'_0, ζ'_0 from Eq. (B5) inside Eq. (41) yields

$$\lambda_{\pm}^2 = \mathcal{A}^2\cosh^2(\kappa'_w X'_0)\,\frac{c^2K'^2\kappa_w'^2}{\Omega'^2}\left[1 \pm \frac{\gamma_u\omega_b^2}{c^2\kappa_w'^2\mathcal{A}\cosh(\kappa'_w X'_0)} \pm \frac{a_w^2}{\mathcal{A}}\,\frac{\cosh(2\kappa'_w X'_0)}{2\cosh(\kappa'_w X'_0)}\right]. \tag{42}$$

Assume for the moment positive detuning $\Delta_\omega > 0$. Then the right hand side with $(+)$ is definitely positive; the eigenvalues λ_+ are always real, hence the fixed point at $k'_{rz}\Psi'_0 = +\pi/2 + k'_{rx}X'_0$ is always *unstable*. The eigenvalues for the other fixed point at $k'_{rz}\Psi'_0 = -\pi/2 - k'_{rx}X'_0$ change from real to pure imaginary when H_{XX} changes sign. That transition occurs for radiation power

$$\mathcal{A} < a_w^2\,\frac{\cosh(2\kappa'_w X'_0)}{2\cosh(\kappa'_w X'_0)} + \frac{\gamma_u\omega_b^2}{c^2\kappa_w'^2\cosh(\kappa'_w X'_0)} \tag{43}$$

The combined effect of the wiggler strength variation and the space charge induced velocity shear is the formation of trapped particle islands at low radiation power. Similar conclusions apply in case of negative detuning $\Delta_\omega < 0$, where the generically unstable point is now located at $k'_{rz}\Psi = -\pi/2 - k'_{rx}X'_0$.

Consider the efficiency in the deeply trapped parameter range, where the $\ll$ applies in Eq. (43). The maximum excursion δX equals the island height, given by

$$\Delta X \simeq \sqrt{\frac{2mc^2\mathcal{A}\cosh(\kappa'_w X'_0)}{|H'_{XX}|}}, \tag{44}$$

where it has been assumed $X_0^+ \simeq X_0^- \simeq X'_0$ for the X locations of the stable and unstable fixed points at $k'_{rz}\Psi = \pm\pi/2$. Using the approximation (B5) for H'_{XX} in the deeply trapped region and neglecting the space-charge contribution from ω_b^2,

$$\Delta X \simeq \frac{1}{\kappa'_w}\,\sqrt{\frac{4\mathcal{A}}{a_w^2}\,\frac{\cosh(\kappa'_w X'_0)}{\cosh(2\kappa'_w X'_0)}}. \tag{45}$$

It follows that the efficiency (32) is of the order

$$\eta \simeq 2\,\frac{\Delta X}{D}\,\frac{V_0}{V_b} = \frac{V_0}{V_b}\,\frac{4}{k'_w D}\,\sqrt{\frac{\mathcal{A}}{a_w^2}\,\frac{\cosh(\kappa'_w X'_0)}{\cosh(2\kappa'_w X'_0)}}, \tag{46}$$

where, for small η, the denominator in Eq. (32) was taken as unity. Both the island height and the efficiency scale as $\sqrt{a_r}/a_w$.

We now seek the relation between efficiency and the bounce frequency,

$$\Omega'_b = |\lambda| = \frac{1}{m\Omega'}\,\sqrt{mc^2\mathcal{A}\cosh(\kappa'_w X'_0)K'^2|H_{XX}|}, \tag{47}$$

where the deeply trapped region approximation (B6) was applied to $|H_{X\Psi}^2 - H'_{XX}H'_{\Psi\Psi}|$ inside the root. Given that the optimum grating length is half a bounce period in the laboratory frame $L_w = u(\pi/\Omega_b)$, where $\Omega_b = \Omega'_b/\gamma_u$, one has

$$L_w = \pi\,\frac{c\Omega'}{K'}\,\frac{m\gamma_u\beta_u}{\sqrt{mc^2\mathcal{A}\cosh(\kappa'_w X'_0)|H'_{XX}|}}. \tag{48}$$

Expressing $|H'_{XX}|$ in terms of L_w from Eq. (48), and substituting for ΔX in Eqs. (44) and (46) yields

$$\eta \simeq \frac{V_0}{V_b}\frac{\sqrt{2}\pi}{(\kappa_w' D)(\kappa_w' L_w)}\frac{\Omega'}{cK'} \times \frac{1}{\sqrt{(a_w^2/2)\cosh(2\kappa_w' X_0') + \gamma_u(\omega_b^2/c^2\kappa_w'^2)}}. \quad (49)$$

Hence, in the low power, trapped particle regime, the DEL efficiency scales inversely proportional to the grating length L_w, just as in an FEL.

The factor multiplying $1/k_w L_w$ in the right-hand side of Eq. (49) can be larger than unity, tempting the thought that η is higher than the analogous FEL expression $\eta^* = \pi/k_w L_w$. It is, but expression (49) cannot be used for direct comparisons with FEL efficiency because the optimum DEL length, half-bounce period L_w, is not the same as the optimum FEL length L_w of the same parameters. A direct comparison between the FEL efficiency, written for $\gamma_u \gg 1$ as

$$\eta^* = 2\frac{\gamma_u mc^2}{eV_b}\sqrt{a_w a_r}, \quad (50)$$

where $eV_b = (\gamma_u - 1)mc^2$, and Eq. (46), yields

$$\frac{\eta}{\eta^*} \simeq \frac{1}{k_w' D}\frac{eV_0}{mc^2}\frac{2}{a_w^{3/2}}\begin{pmatrix}\sqrt{\sin\phi/\gamma_\perp'\beta_u}\\ \sqrt{\cos\phi/\gamma_\perp'}\end{pmatrix}\sqrt{\frac{\cosh(k_w' X_0')}{\cosh(2k_w' X_0')}}. \quad (51)$$

for ES and EM wigglers, respectively. At moderate wiggler strengths $a_w < 1$, low power DEL operation remains more efficient than an FEL because the DEL trapped particle excursions, scaling as $1/a_w$ on the wiggler strength, are much larger than those in an FEL that scale as $a_w^{1/2}$.

The tendency for higher than $1/2N_w$ efficiency at lower wiggler strength is illustrated in Fig. 8, plotting efficiency vs interaction length at low radiation power $a_r = 0.002$, and for $\mathcal{V}_0/V_b = 2$ inside an A-K gap $k_w D = 2.25$. At $a_w = 0.50$ (solid curve) the maximum $\eta = 0.015$ approximately equals $\frac{1}{60}$, where $2N_w = 60$ is the bounce period estimated from the curve. The optimum efficiencies at progressively lower $a_w = 0.30$ and $a_w = 0.15$ increase to $\eta = 0.055$ and $\eta = 0.080$, much higher than $1/2N_w$ with, respectively, $2N_w = 50$ and $2N_w = 120$ (estimated from the same curves). DEL operation may have advantages in the case of EM wigglers, where the wiggler strength is typically small, $a_w \leqslant 10^{-2}$.

VI. TAPERING AND SENSITIVITY TO THERMAL SPREADS

The discussion so far dealt with radiation of uniform cross section da_r/dX, as, for example, in case of TE_{n0} mode excitation in rectangular wave guides. Two issues are raised in quasioptical (Fabry-Perot) resonators, when radiation of a finite cross-section envelope $w_0 \leqslant D$ is considered: (a) loss of the beam-radiation overlap after some interaction length z due to the off-axis shift $\langle \delta X \rangle$ of the beam and (b) reduction in efficiency, caused by thermal spreads of the injected GC location.

The sensitivity to thermal spreads is addressed first. Application of the canonical momentum conservation between two points of an electron orbit located inside and far outside the wiggler (where $E_0 = B_0 = 0$) shows that an initial mismatch from the exact $E_0 \times B_0$ factor γ_u,

$$\delta\gamma \equiv \gamma - \gamma_u \simeq \gamma_u^3 \beta_u^2 \delta v_y, \quad \delta v_y \equiv v_y - u, \quad (52)$$

causes a GC shift δX from the intended location, given by

$$\delta X = \frac{\delta\gamma u + \gamma_u \delta v_y}{\Omega} \simeq \gamma_u \beta_u \frac{c}{\Omega}\frac{\delta\gamma}{\gamma_u} \quad (53)$$

(the correction from $\delta v_x \equiv v_x$ is of order δv_x^2 and is neglected). The excess energy is converted into cyclotron rotation. Applying energy conservation $mc^2\gamma_u\gamma_\perp = mc^2\gamma_{u+\delta v}$, where $\gamma_\perp \simeq 1 + \Omega^2\rho^2/2\gamma_u^2 c^2$ and we assumed negligible potential difference along the beam direction z, the Larmor radius is given by

$$\rho = \gamma_u \frac{c}{\Omega}\left(\frac{2\delta\gamma}{\gamma_u}\right)^{1/2}. \quad (54)$$

To maintain good overlapping with radiation one must limit δX, ρ well below the radiation waist w_0, and/or the gap size D. From Eqs. (53) and (54) $\rho \geqslant \delta X$, hence the tolerance to thermal spreads is determined by the condition $\rho/D \ll 1$, or

$$\frac{\delta\gamma}{\gamma_u} \ll \left(\frac{D\Omega}{c}\right)^2 \frac{1}{2\gamma_u^2}. \quad (55)$$

The right-hand side limit is given by $1.72\, B^2[\mathrm{T}]\, D^2[\mathrm{cm}]/\gamma_u^2$ and allows a much more relaxed beam quality constraint than its FEL counterpart, given by

$$\frac{\delta\gamma}{\gamma_u} \ll \frac{1}{2N_w}. \quad (56)$$

In a DEL, the velocity or energy spreads of the injected beam are converted into spreads in the GC location affecting the overlap in real space. The velocity mismatch *per se*, which causes detuning in an FEL, is irrelevant here since the GC's of all electrons drift at the same u. Notice that in a DEL the required beam quality is not affected by the wiggler length as in an FEL.

Premature saturation due to the beam slipping outside the radiation envelope, as the electrons drift upwards in X, is now addressed. One intuitively anticipates that overlapping with the radiation can still be maintained if the radiation beam is tilted relative to the drift direction, accomplished by tilting the resonator by a small angle θ. The emission angle $\phi = \theta$ will then be naturally selected through the tilt. Because $\delta\langle X \rangle$ is related to the radiated power through Eq. (33), one can relate the tilt $\theta = \tan^{-1}(\delta\langle X\rangle/L)$ to the per-pass resonator gain $G = \delta P_r/P_c = 1/Q$, with

$$\theta = \tan^{-1}\left(\frac{\Delta P_r}{I_b V_0}\frac{2D}{L}\right) = \tan^{-1}\left(G\,\frac{P_c}{I_b V_0}\frac{2D}{L}\right), \quad (57)$$

P_c being the circulating radiation power and Q the cavity quality factor. However, one must still ensure that the gradients in the radiation strength da_r/dX do not change significantly the nature of the particle motion.

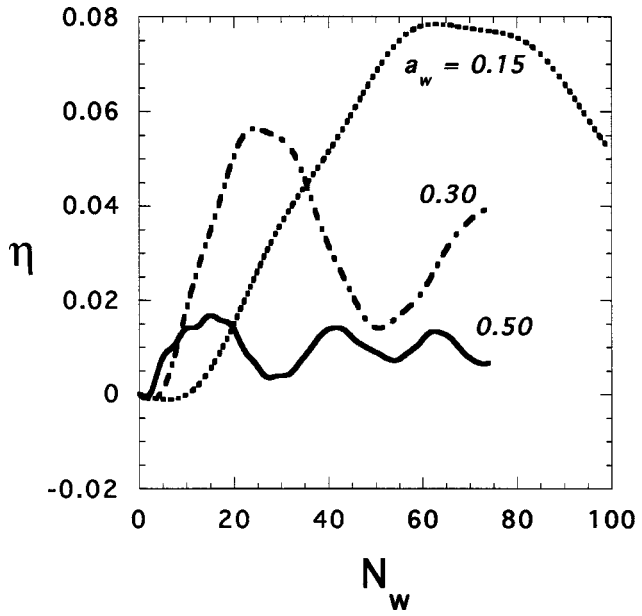

FIG. 8. Sheet beam efficiency vs number of wiggler periods at low radiation power $a_r=0.002$, for $\mathcal{V}_0/V_b=2$, $k_wD=2.25$, $u/c=0.99$. Various curves correspond to different wiggler strengths a_w, as marked.

To include the effects of the finite radiation spot size, a Gaussian beam of waist w_0 is assumed. The new slow time scale Hamiltonian is obtained from Eq. (26) by replacing

$$a_r \rightarrow a_r(X') \equiv a_{r\sigma}\exp\left[-\frac{(X'-d)\cos\phi - Z'\sin\phi]^2}{w_0^2}\right], \tag{58}$$

for an optical beam entering the resonator at $X'=d$ and propagating at an angle ϕ. In the parallel limit $\phi=0$ the new orbits are given by $H=\text{const}$, where

$$H_R' = mc^2\overline{\gamma_\perp'} + \mathcal{A}e^{-(X'-d)^2/w^2}\cosh(\kappa_w' X') \times \sin(K'\Psi' + k_{rx}' X') - \frac{\Delta_\omega'}{K'} m\Omega' X', \tag{59}$$

and the slow phase variation of the Gaussian beam has been neglected. The gradient da_r/dX' changes the particle orbits; it has been shown [1] that the orbits become trapped inside islands when the waist size falls below

$$w_0 < w_{\rm cr} = \sqrt{2(1+\xi^2)}\,\frac{\lambda_w}{2\pi}. \tag{60}$$

In that case the maximum excursion is limited by the radiation waist w. The general case of oblique emission $\phi\neq 0$ is not amenable to exact analysis because we can no more eliminate the time dependence and consider H_R' an invariant of the motion [Z' in Eq. (58) depends explicitly on both Ψ' and t']. If the Z' dependence is simply dropped from the Gaussian exponent for $\sin\phi \sim 1/\gamma_u^2 \ll 1$ one obtains the orbits illustrated in Fig. 8. In Fig. 9(a) the waist w_0 is below the limit (60) leading to island formation; the island disappears and unbound motion returns in Fig. 9(b), where the waist

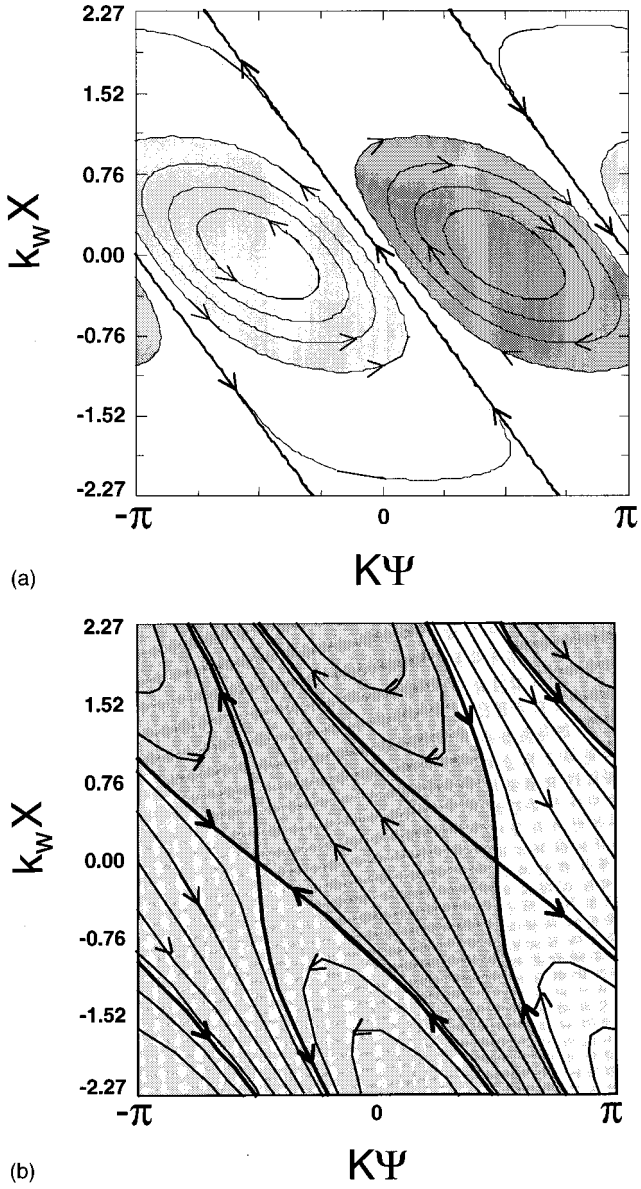

FIG. 9. Effect of a finite radiation cross section on the GC orbits at zero detuning $\xi=0$ and Gaussian waist size of (a) $k_ww_0=75$ and (b) $k_ww_0=250$.

size w_0 is above $w_{\rm cr}$. Hence the spot-size criterion, obtained for $\phi=0$, holds approximately for small ϕ. The conclusion is confirmed by numerical integration of the GC equations of motion with the full Z' dependence in the Gaussian.

VII. CONCLUSIONS

Comparison between the ES wiggler results derived here, with the corresponding MS wiggler results in Ref. [1] shows that (a) for equal wiggler strengths $E_w=B_w$ the radiated power in the ES case is modified by the factor $\beta_u\gamma_u^2\sin\phi$, (b) the emission angle ϕ affects the detuning ξ at given wiggler-radiation strengths, and (c) for given detuning, the trapped particle fraction and efficiency are independent of the emission angle. Hence the MS and ES versions operate at the same efficiency for the same detuning when $\sin\phi=1/\gamma_u^2\beta_u$.

High power operation of a DEL amplifier using either a ES or MS wiggler has the following advantages over an FEL with the same operation parameters: (a) much higher efficiency that is not limited by wiggler length, (b) higher gain per wiggler period owing to the nature of the particle acceleration, and (c) lower sensitivity to the beam thermal spreads.

For the high-efficiency mode, the radiation strength much exceed the shear effects from the wiggler gradient and the beam space charge. The space charge effects, in the far right-hand side of Eq. (43), are less important than the wiggler gradient for beam current densities of

$$J_b[A/\mathrm{cm}^2] \leqslant 0.205\gamma_u\beta_u^3 V_w^2[\mathrm{kV}]/\lambda_w^2[\mathrm{cm}],$$

$$J_b[A/\mathrm{cm}^2] \leqslant 0.205\gamma_u^{-1}\beta_u A_w^2[\mathrm{kV}]/\lambda_w^2[\mathrm{cm}], \qquad (61)$$

for the ES and MS wiggler. For current densities below Eq. (61) one must overcome only the wiggler gradient term in Eq. (43). Apart from geometric factors of order unity, the circulating power must be above

$$P_r[MW] \geqslant 4.3\times 10^4 a_w^2 (r/\lambda_r)^2, \qquad (62)$$

r being the spot-size radius, in order to achieve high efficiency with unbound excursions. High efficiency favors low strength wigglers; a drawback in that case is the increased start-up current.

For operation at power levels below Eq. (62), the DEL efficiency in the trapped island configuration, though scaling inversely proportional to the wiggler length, can nevertheless be higher than the $1/2N_w$ FEL limit. Operation as an oscillator, starting up from noise, can still have an advantage over an FEL, particularly in the low wiggler strength regime. An important application can be tabletop DEL operation with EM wigglers where a_w is inherently low.

Tapering in a DEL means maintaining the overlapping in space between the radiation and the off-axis shifting electrons, and is accomplished simply by tilting the resonator axis (in an FEL, by contrast, one must vary the wiggler parameters to maintain the resonance between electron velocities and phase velocity). The tilt angle (57) is small, falling within the spontaneous emission cone $\theta \leqslant 1/\gamma_u$, so the device can start up from noise. For operation with TE_{0m} wave guide modes, where the radiation amplitude is uniform across the beam, no tapering is required.

Unlike an FEL where the efficiency is limited by the interaction physics, the DEL efficiency is only limited by technology, meaning the maximum sustainable voltage in the anode-cathode gap. The DEL efficiency η, for optimum beam placement $k_w d^* = 0.7$, is plotted as a function of the beam energy and the upshifting factor $\beta_u(1+\beta_u)\gamma_u^2$ in Figs. 10(a) and 10(b), respectively. Different curves correspond to different values of the maximum voltage V_0 that can be sustained over a 1 cm gap. The lowest curve represents todays state-of-the-art value of 1 MV/cm. The highest efficiency occurs at low beam energies and low upshifting factors; the DEL scheme is ideally suited for tabletop microwiggler devices. Even so, efficiency over 10% can be achieved at upshifting factor 100; the corresponding untapered FEL limit for 50 wiggler periods is just 1%. An even larger efficiency payoff by pushing the voltage breakdown limit to 3 and 5 MV/cm is evident in Fig. 10.

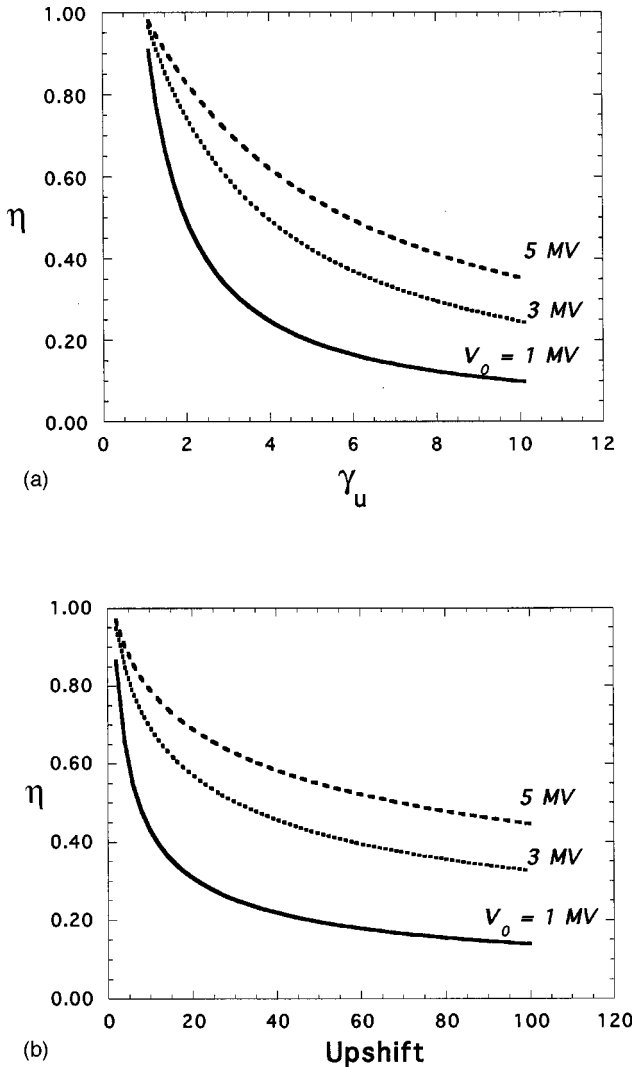

FIG. 10. Maximum efficiency η as a function (a) of the beam energy and (b) the upshifting factor $U=\beta_u(1+\beta_u)\gamma_u^2$, for different values of the maximum voltage V_0 that can be sustained over a 1 cm gap.

APPENDIX A: COMPUTATION OF THE RESONANT INTERACTION HAMILTONIAN

The Hamiltonian is expressed in the GC coordinates by substituting Eq. (20) inside Eqs. (18) and (19) with the fields given by Eqs. (13) and (14). The leading order undulation, Eq. (18), becomes

$$H_0'(I',\theta',X',Z')=mc^2\Bigg\{\sqrt{1-2\frac{\Omega' I'}{mc^2}}+\gamma_u\left(\frac{eV_w}{mc^2}\right)\sum_{N=0}^{\infty}Q_N(X',\rho')\cos[k_w'Z'+N\theta'-\omega_w't'+\alpha_N]$$
$$+\gamma_u\beta_u\sin\phi\left(\frac{eA_r}{mc^2}\right)\sum_{m=-\infty}^{\infty}\sum_{n=-\infty}^{\infty}J_m(k_{rx}'\rho')J_n(k_{rz}'\rho')\sin\left[k_{rx}'X'+k_{rz}'Z'+(m+n)\theta'-\omega_r't'+n\frac{\pi}{2}\right]\Bigg\}, \tag{A1}$$

where $\beta_u=u/c$, $\beta_\perp'=\Omega'\rho'/c$, $\rho'=\sqrt{-2I'/\Omega'}$ (here the action I' is negative due to the electron counter-rotation),

$$Q_n(X',\rho')=h_n(\kappa_w'\rho')\cosh(\kappa_w'X')-q_n(\kappa_w'\rho')\sinh(\kappa_w'X'), \tag{A2}$$

and the expansion coefficients $h_n(\kappa_w'\rho')$, $q_n(\kappa_w'\rho')$ scale as $q_n\sim h_n\sim(k_w'\rho')^n$ and are given by

$$\left.\begin{aligned}h_n(\rho)&=\sum_{j=\text{even}}(-1)^{j/2}I_{n-j}(\rho)J_j(\rho),\\ q_n(\rho)&=\sum_{j=\text{odd}}(-1)^{(j+1)/2}I_{n-j}(\rho)J_j(\rho),\end{aligned}\right\}\quad\alpha_n=0,\quad n\ \text{even},$$
$$\left.\begin{aligned}h_n(\rho)&=\sum_{j=\text{odd}}(-1)^{(j+1)/2}I_{n-j}(\rho)J_j(\rho),\\ q_n(\rho)&=\sum_{j=\text{even}}(-1)^{j/2}I_{n-j}(\rho)J_j(\rho),\end{aligned}\right\}\quad\alpha_n=\frac{\pi}{2},\quad n\ \text{odd}, \tag{A3}$$

with the properties $h_n(\rho)=h_{-n}(\rho)$, $q_n(\rho)=-q_{-n}(\rho)$ (the last means $q_0\equiv 0$).

We want to eliminate the fast oscillating terms from Eq. (A1) considering operation far from resonances between the wiggling and the cyclotron motion, i.e., $d/dt(k_w'Z'-\omega_w't'+n\theta')\neq 0$. To that end we introduce the new averaged variables $\overline{X'},\overline{Z'}$ through the canonical transformation

$$\overline{X'}=X'+\epsilon\frac{\partial S_1}{\partial(m\Omega'\overline{Z'})},\quad \overline{Z'}=Z'-\epsilon\frac{\partial S_1}{\partial(m\Omega' X')},$$
$$\overline{H_0'}=H_0'+\frac{\partial S_1}{\partial t'}, \tag{A4}$$

where a_r,a_w are $O(\epsilon)$. The generating function $S_1(\overline{Z'},X',t')$ is chosen so as to kill fast varying terms to order ϵ upon substitution of Eq. (A1) inside Eq. (A4); hence, from

$$\frac{\partial S_1}{\partial t'}+H_0'(X',\overline{Z'})=mc^2\gamma_\perp' \tag{A5}$$

follows

$$S_1=-mc^2\frac{\gamma_u}{\omega_w'}\left(\frac{eV_w}{mc^2}\right)\sum_{N=0}^{\infty}Q_N(X',\rho')\sin[k_w'\overline{Z'}+N\theta'-\omega_w't'+\alpha_N]$$
$$-mc^2\frac{\gamma_u\beta_u}{\omega_r'}\sin\phi\left(\frac{eA_r}{mc^2}\right)\sum_{m=-\infty}^{\infty}\sum_{n=-\infty}^{\infty}J_m(k_{rx}'\rho')J_n(k_{rz}'\rho')\cos\left[k_{rx}'X'+k_{rz}'\overline{Z'}+(m+n)\theta'-\omega_r't'+n\frac{\pi}{2}\right]. \tag{A6}$$

Thus, expressing H_0' in terms of the averaged $\overline{X'},\overline{Z'}$ and expanding according to Eqs. (A4) and (A5) yields

$$\overline{H_0'}(\overline{X'},\overline{Z'})=mc^2\sqrt{1-2\frac{\Omega' I'}{mc^2}}+O(\epsilon^2)=mc^2\sqrt{1+\beta_\perp'^2}. \tag{A7}$$

The Larmor radius and cyclotron frequency are constant to order ϵ. To that order, the fast-time averaged GC location is also fixed in the drifting frame since $d\overline{X'}=\partial\overline{H_0'}/\partial(m\Omega'\overline{Z'})=0$, $d\overline{Z'}=-\partial\overline{H_0'}/\partial(m\Omega'\overline{X'})=0$. The transformation killed the fast variation to order ϵ; it, however, introduced second order fast-beating terms

$$\frac{1}{m\Omega'}\left[\frac{\partial\overline{H_0'}}{\partial d\overline{X'}}\frac{\partial S_1'}{\partial\overline{Z'}}-\frac{\partial\overline{H_0'}}{\partial\overline{Z'}}\frac{\partial S_1'}{\partial\overline{X'}}\right], \tag{A8}$$

to be considered with H_1'.

Finite, slow GC displacement comes from the second order interaction, through the ''beating'' between the wiggling motion and the radiation. Expansion of the electromagnetic interaction term H_1, Eq. (19), in cyclotron harmonics yields, after certain rearrangements

$$\begin{aligned}
H_1'=&mc^2\left(\frac{eA_r}{mc^2}\right)\frac{\beta_\perp'}{\gamma_\perp'}(\cos\theta'\cos\phi-\gamma_u\sin\theta'\sin\phi)\sum_{m=-\infty}^{\infty}\sum_{n=-\infty}^{\infty}J_m(k_{rx}'\rho')J_n(k_{rx}'\rho')\cos[k_{rx}'X'+k_{rz}'Z'+(m+n)\theta'-\omega_w't']\\
&+mc^2\left(\frac{eV_w}{mc^2}\right)\beta_u\gamma_u\frac{\beta_\perp'}{\gamma_\perp'}\sin\theta'\sum_{N=0}^{\infty}Q_N(X',\rho')\cos[k_w'Z'+N\theta'-\omega_w't'+\alpha_N]-\frac{mc^2}{\gamma_\perp'}\left(\frac{eA_r}{mc^2}\right)\\
&\times\left(\frac{eV_w}{mc^2}\right)\gamma_u^2\beta_u\sin\phi\frac{1}{2}\sum_{m=-\infty}^{\infty}\sum_{N=0}^{\infty}J_m(k_{rx}'\rho')Q_N(X',\rho')\{\cos[k_{rx}'X'+(k_{rz}'+k_{rw}')Z'+(m+N)\theta'-(\omega_r'+\omega_w')t'+\alpha_N]\\
&-\cos[k_{rx}'X'+(k_{rz}'-k_{rw}')Z'+(m-N)\theta'-(\omega_r'-\omega_w')t'+\alpha_N]\}+\frac{1}{8}mc^2\gamma_u^2\sin^2\phi\left(\frac{eA_r}{mc^2}\right)^2\\
&\times\left\{1-\sum_{m=-\infty}^{\infty}\sum_{n=-\infty}^{\infty}J_m(2k_{rx}'\rho')J_n(2k_{rz}'\rho')\sin\left[2k_{rx}'X'+2k_{rz}'Z'+(m+n)\theta'-2\omega_r't'+n\frac{\pi}{2}\right]\right\}+\frac{1}{8}mc^2\gamma_u^2\beta_u^2\left(\frac{eA_w}{mc^2}\right)^2\\
&\times\left\{1+i^m\sum_{m=-\infty}^{\infty}\sum_{n=-\infty}^{\infty}I_m(2\kappa_w'\rho')J_n(2k_w'\rho')\cos\left[2ik_w'X'+2k_w'Z'+(n+m)\theta'-2\omega_w't'+n\frac{\pi}{2}\right]\right\}.
\end{aligned} \tag{A9}$$

Here, since H_1' is already of second order, one simply substitutes $\overline{X'}\simeq X'$, $\overline{X'}\simeq X'$ inside Eq. (A9). The first double sum comes from the interaction of the cyclotron rotation with the radiation and the second sum comes from the interaction of the cyclotron rotation with the undulation. None of the above contains the coupling k_w+k_r characteristic of the FEL emission; they both correspond to emission at Doppler shifted cyclotron frequencies, Eq. (11), far from the DEL operation frequency. It is the third sum that contains the ''beating'' of the wiggling motion with the radiation, and leads to emission at the upshifted wiggler as well as upshifted wiggler-cyclotron harmonics, Eq. (12). Finally the last two sums contain harmonics of the radiation and the undulation frequency, respectively.

The slow motion near the DEL frequency, up to order ϵ^2, is obtained by just dropping the fast oscillating terms, eliminating all but the third sum from Eq. (A9). In addition, one must take the $k_w'\rho'\sim k_r'\rho'\sim\epsilon$ limit since the Larmor radius must be smaller than the anode-cathode gap D, of the order of the wiggler period, $\rho'/D\sim 2\pi/k_w'\ll 1$. Thus only the $m=n=N=0$ terms, of order ϵ^0 survive in the remaining sums inside Eq. (A9). Letting $Q_0\to\cosh(\kappa_w'X')$ as $J_0I_0\to 1-(1/4)(\kappa_w'\rho')^4$ yields

$$\begin{aligned}
H_1'\simeq&-\frac{mc^2}{\gamma_\perp'}\left(\frac{eA_r}{mc^2}\right)\left(\frac{eV_w}{mc^2}\right)\gamma_u^2\beta_u\sin\phi\cosh(\kappa_w'X')\{\cos[k_{rx}'X'+(k_{rz}'+k_{rw}')Z'-(\omega_r'+\omega_w')t']-\cos[k_{rx}'X'-(k_{rz}'-k_{rw}')Z'-(\omega_r'\\
&-\omega_w')t']\}+\frac{1}{8}mc^2\left\{\gamma_u^2\sin^2\phi\left(\frac{eA_r}{mc^2}\right)^2+\gamma_u^2\beta_u^2\left(\frac{eA_w}{mc^2}\right)^2(1+\cosh[2k_w'X'])\right\}.
\end{aligned} \tag{A10}$$

Only the $(+)$ sign term $(k_r'+k_w')$, corresponding to emission at upshifted frequency is kept; the $(-)$ terms $(k_r'-k_w')$ correspond to emission of downshifted frequency and are out of resonance. Finally, and for the same reason, we discard the terms (A8) introduced by the transformation, since their harmonic expansion contains only k_r-k_w,

$$\begin{aligned}
-(mc^2)^2\gamma_u^2\beta_u\sin\phi&\left(\frac{eA_r}{mc^2}\right)\left(\frac{eV_w}{mc^2}\right)\sum_{m=-\infty}^{\infty}\sum_{n=-\infty}^{\infty}\sum_{N=0}^{\infty}\left\{J_m(k_{rx}'\rho')J_n(k_{rz}'\rho')Q_N(X',\rho')\frac{k_{rx}'k_w'}{m\Omega'\omega_w'}\cos[k_{rx}'X'-(k_{rz}'-k_{rw}')Z'-(\omega_r'\right.\\
&\left.-\omega_w')t']+J_m(k_{rx}'\rho')J_n(k_{rz}'\rho')P_N(X',\rho')\frac{k_{rz}'\kappa_w'}{m\Omega'\omega_w'}\sin[k_{rx}'X'-(k_{rz}'-k_{rw}')Z'-(\omega_r'-\omega_w')t']\right\}.
\end{aligned} \tag{A11}$$

Thus combining Eq. (A10) with the zeroth-order Eq. (A2) yields the resonant (DEL) interaction Hamiltonian

$$H_R' = mc^2\sqrt{1-2\frac{\Omega' I'}{mc^2}+\frac{1}{4}\gamma_u^2\beta_u^2\left(\frac{eA_w}{mc^2}\right)^2(1+\cosh[2k_w'X'])} - \frac{mc^2}{\gamma_\perp'}\left(\frac{eA_r}{mc^2}\right)\left(\frac{eV_w}{mc^2}\right)\gamma_u^2\beta_u\sin\phi\cosh(\kappa_w'X')$$
$$\times\cos[k_{rx}'X'+(k_{rz}'+k_{rw}')Z'-(\omega_r'+\omega_w')t'].\tag{A12}$$

The ''ponderomotive phase'' ψ' is given by

$$\psi' \equiv (k_{rz}'+k_w')Z'+k_{rx}'X'-(\omega_r'+\omega_w')t'.\tag{A13}$$

The slow phase variation near resonance is characterized by $d\psi'/dt' \ll \omega_r'$. Since the time-scale separation already implies slow GC motion in the drifting frame $(k_{rz}'+k_w')dZ'/dt' \sim k_{rx}'dX'/dt' \ll \omega_\tau'$, the total time derivative of Eq. (28) yields the resonant condition $\omega_\tau'+\omega_w' \simeq 0$. In the lab frame coordinates that yield Eq. (5) are in the form

$$\psi_r(1-\beta_u\cos\phi)-k_w u = 0.\tag{A14}$$

Finally we eliminate the explicit time dependence by defining $\Psi' = Z'-(\omega_r'+\omega_w')t'/(k_{rz}'+k_w')$ as the new ''position'' in place of Z'; its new conjugate coordinate remains the same $\chi = X'$ and the transformed resonant Hamiltonian becomes

$$H_R' = mc^2\overline{\gamma_\perp'}+\frac{mc^2 a_w a_r}{2\overline{\gamma_\perp'}}\gamma_u^2\beta_u\sin\phi\cosh(\kappa_w'X')$$
$$\times\sin(K'\Psi'+k_{rx}'X')-\frac{\Delta_\omega'}{K'}m\Omega' X',\tag{A15}$$

$$\overline{\gamma_\perp'}(X') = \sqrt{1-2\frac{\Omega' I'}{mc^2}+\overline{a_w^2}(X')}$$
$$= \sqrt{1+\frac{\Omega'^2\rho'^2}{mc^2}+\overline{a_w^2}(X')},$$

$$\overline{a_w^2}(X') = \frac{1}{4}\gamma_u^2\beta_u^2\left(\frac{eA_w}{mc^2}\right)^2(1+\cosh[2k_w'X'])$$
$$+\frac{1}{4}\gamma_u^2\sin^2\phi\left(\frac{eA_r}{mc^2}\right)^2,\tag{A16}$$

where

$$K' \equiv k_w'+k_{rz}' \simeq 2k_w', \quad \Delta_\omega' \equiv \omega_r'+\omega_w'.\tag{A17}$$

To estimate mode competition, the closest resonant interaction to the fundamental DEL frequency is the hybrid wiggler-cyclotron frequency, Eq. (12), described by the following part of Eq. (A9):

$$\frac{mc^2}{\gamma_\perp'}\left(\frac{eA_r}{mc^2}\right)\left(\frac{eV_w}{mc^2}\right)\gamma_u^2\beta_u\sin\phi[J_1(\kappa_w'\rho')Q_0(X',\rho')$$
$$+J_0(\kappa_w'\rho')Q_1(X',\rho')]\{\sin[k_{rx}'X'+(k_{rz}'+k_{rw}')Z'+\theta'$$
$$-(\omega_r'+\omega_w')t']-\sin[k_{rx}'X'-(k_{rz}'-k_{rw}')Z'+\theta'$$
$$-(\omega_r'-\omega_w')t']\}.\tag{A18}$$

Therefore the interaction strength at a frequency displaced by the nth cyclotron harmonic is smaller than the DEL carrier by $J_n \sim Q_n \sim (\kappa_w'\rho')^n$ [notice that Eq. (A18) is also smaller than the usual cyclotron maser interaction strength $dJ_n/dr \sim (\kappa_w'\rho')^{n-1}$].

APPENDIX B: FIXED POINTS

When the full space charge and wiggler gradient effects are retained, the fixed points, zeros of the equations of motion (29a) and (29b), are given by

$$k_{rz}'\Psi_0'+k_{rx}'X_0' = \pm\frac{\pi}{2},$$

$$mc^2\left[\kappa_w'\frac{a_w^2}{4}\cosh(2\kappa_w'X_0')\pm\mathcal{A}\sinh(\kappa_w'X_0')\right]$$
$$=\gamma_u m\omega_b^2 X_0'-\frac{m\Delta_\omega'\Omega'}{K'}.\tag{B1}$$

Defining $\sinh(k_w'X_0') \equiv \xi$ yields the solution

$$\xi = \pm\frac{\sinh^{-1}\xi(\gamma_u\omega_b^2/\kappa_w'^2c^2)-\Delta_\omega'\Omega'/K'\kappa_w'c^2}{\mathcal{A}\mp(1/2)a_w^2\sqrt{1+\xi^2}}.\tag{B2}$$

Expression (B2) is reduced to Eq. (34) in the small space charge, small wiggler strength limit $a_w, \omega_b^2/\kappa_w'^2c^2 \ll 1$. The derivatives at X_0', Ψ_0' are given by

$$H_{X\Psi}' = \mp mc^2K'k_{rx}'\mathcal{A}\cosh(\kappa_w'X_0'),$$
$$H_{\Psi\Psi}' = \mp mc^2K'^2\mathcal{A}\cosh(\kappa_w'X_0'),\tag{B3}$$

$$H_{XX}' = \pm mc^2\kappa_w'^2\left[\left(1-\frac{k_{rx}'^2}{\kappa_w'^2}\right)\mathcal{A}\cosh(\kappa_w'X_0')\mp\gamma_u\frac{\omega_b^2}{\kappa_w'^2c^2}\right.$$
$$\left.\mp\frac{a_w^2}{2}\cosh(2\kappa_w'X_0')\right],\tag{B4}$$

Substituting into Eq. (41) yields Eq. (42). In the deeply trapped region $a_r a_w \ll a_w^2, (\omega_b/c\kappa_w')^2$, the factor H_{XX}' is approximated by

$$|H_{XX}'| = mc^2\kappa_w'^2\left[\frac{a_w^2}{2}\cosh(2\kappa_w'X_0')+\gamma_u\frac{\omega_b^2}{c^2\kappa_w'^2}\right].\tag{B5}$$

independent of A_r. Also, in the deeply trapped region

$$|H_{X\Psi}^2 - H_{XX}'H_{\Psi\Psi}'| \simeq mc^2\mathcal{A}\cosh(\kappa_w'X_0')K'^2H_{XX},\tag{B6}$$

where the right-hand side appears in the bounce period (47).

[1] S. Riyopoulos, Phys. Plasmas **B3**, 3828 (1996).
[2] S. Riyopoulos, Nucl. Instrum. Methods Phys. Res. (to be published).
[3] H. Motz, J. Appl. Phys. **22**, 527 (1951).
[4] J. M. J. Madey, J. Appl. Phys. **42**, 1906 (1971).
[5] W. B. Colson, IEEE J. Quantum Electron. **QE17**, 1417 (1981).
[6] See, for example, T. C. Marshall, in *Free-electron Lasers* (McMillan, New York, 1985), and references therein.
[7] S. Riyopoulos, Phys. Rev. E **55**, 1876 (1997).
[8] E. Ott and W. M. Manheimer, IEEE Trans. Plasma Sci. **3**, 1 (1975).
[9] See, for example, *Microwave Magnetrons*, edited by G. B. Collins (McGraw-Hill, New York, 1948), and references therein.
[10] S. Riyopoulos, IEEE Trans. Plasma Sci. **22**, 626 (1994).
[11] S. Riyopoulos, IEEE J. Quantum Electron. **31**, 1579 (1995).
[12] In the drifting frame the emitted radiation emerges at an angle $\phi' > \phi$ relative to the drift direction, according to

$$\tan\phi' \equiv \frac{k'_{rx}}{k'_{rz}} = \frac{\tan\phi}{\gamma_u[1-\beta_u(1/\cos\phi)]} \geqslant 2\gamma_u\tan\phi.$$